Contrib. Astron. Obs. Skalnaté Pleso **56/3**, 68 – 82, (2026)
https://doi.org/10.31577/caosp.2026.56.3.68

DSLR times of minima of selected eclipsing binaries

M. Kamenec, P. Gajdoš and Š. Parimucha

Institute of Physics, Faculty of Science, University of Pavol Jozef Šafárik 040 01 Košice, The Slovak Republic (E-mail: matus.kamenec@student.upjs.sk)

Received: June 23, 2026; Accepted: July 6, 2026

Abstract. We present a collection of eclipse timings of eclipsing binary stars obtained over the extended time interval 2014–2024. In all observations, a DSLR camera was used as the detector. The presented dataset contains 250 previously unpublished minima of 86 eclipsing binary systems obtained at three observing sites. The minima were determined from calibrated light curves using the phenomenological modelling approach, and their uncertainties were estimated by bootstrap resampling. The presented measurements extend the available timing coverage of the observed systems and may contribute to future studies of orbital period variations and other long-term phenomena in eclipsing binaries.

Key words: eclipsing binaries – times of minima – digital single lens reflex – photometry

1. Introduction

The rapid development of digital single-lens reflex (DSLR) cameras since the early 2000s has shown that these instruments are useful not only for astrophotography, but also for photometric measurements of variable stars and exoplanetary transits (e.g. Loughney, 2010; Zhang et al., 2016; Kamenec, 2023). Several studies have confirmed that DSLR sensors can serve as practical alternatives to dedicated CCD and, more recently, CMOS cameras (e.g. Zhang et al., 2016; Kamenec, 2023).

Times of minima are among the most important observational quantities in the study of eclipsing binaries. Long-term collections of eclipse timings allow us to investigate orbital period changes caused by light-time effects due to additional companions (Irwin, 1952), apsidal motion in eccentric binaries (Gimenez & Garcia-Pelayo, 1983), dynamical perturbations in multiple systems (Borkovits et al., 2015), mass-transfer processes, and magnetic activity cycles (Applegate, 1992).

In this paper we present 250 DSLR-based times of minima for 86 eclipsing binary systems, obtained between 2014 and 2024. All reported timings are new and have not been published previously. The observations were carried out mainly at the Kolonica Saddle Observatory and at a private observatory in Prešov, with one additional dataset from the observatory in Valašské Meziříčí. The target list was updated continuously based on target visibility, recommendations from the local variable-star community, and the scientific interest of individual systems. We paid particular attention to eclipsing binaries that are regularly monitored because of suspected or known orbital-period variations reflected in their O–C diagrams. Most of the observed targets are short-period systems, which often made it possible to record both primary and secondary minima in a single night, or to observe minima of several different systems consecutively. Since our main goal was to determine eclipse timings rather than to model the light curves in detail, DSLR cameras turned out to be well suited for this kind of work. Timing measurements do not require high-precision multi-band photometry — the time of minimum can be derived reliably from the shape of the eclipse profile even with moderate photometric accuracy.

2. Observation and data reduction

The observations of minima were either planned in advance or obtained as by-products of observations aimed at constructing phase curves and further analysis of selected systems. Observation planning relied on auxiliary tools, namely PozorWin (Pribulla, private communication) and ephemeris predictions available through the International Variable Star Index (Watson et al., 2007). The instrumental setup evolved over the course of the programme; in total, we used two Newtonian reflectors, and one refractor, as summarised in Tab. 1.

Table 1. Telescope systems used for the observations.

System	Telescope	Mount
I	Newton 150/750 mm	EQ3-2 GoTo
II	Apochromatic refractor 102/500 mm	EQ3-2 GoTo
III	Newton 200/1200 mm	NEQ-6

The observing sites are listed in Tab. 2. Kolonica Saddle lies within the Poloniny Dark Sky Park and offers genuinely dark skies, while Prešov and Valašské Meziříčí are situated in urban residential areas and are affected by moderate light pollution.

All observations were made with an uncooled Canon EOS 500D DSLR camera, equipped with a 15.1-megapixel APS-C CMOS sensor measuring 22.3 × 14.9 mm. The detector has a pixel array of 4752 × 3168 pixels with a pixel size of 4.69 μm and 14-bit analogue-to-digital conversion. Like most DSLR sensors, it is covered by a Bayer filter array of red, green, and blue filters placed over individual pixels. Since this filter array cannot be removed, all photometry was performed in the so-called grayscale (or "clear") mode, in which pixel values are recorded regardless of their Bayer-filter colour, allowing the full sensor area to contribute to the photometric signal (Kamenec, 2023).

Table 2. Observing sites.

Site ID	Site	Country	Coordinates	Alt. [m]	SQM	Bortle class
KOL	Kolonica Saddle	Slovakia	48.936N, 22.274E	441	21.89	3
PO	Prešov	Slovakia	48.974N, 21.261E	248	20.26	5
VM	Valašské Meziříčí	Czechia	49.463N, 17.973E	335	20.73	4

Note. Sky Quality Meter (SQM) values in mag arcsec^{-2} and Bortle class values taken from https://www.lightpollutionmap.info/

Both mount control and image acquisition were managed from a computer. ISO settings and exposure times were adjusted for each target to avoid saturation. The observed stars typically fell in the brightness range 10–12 mag, for which ISO settings of 800–1600 and an exposure time of 30 seconds were used. Images were acquired using one of three software packages — MaximDL[1], Astrophotography Tool[2], or CCDCiel[3] — and stored either in native RAW format or directly as FITS files. The computer clock was synchronized using the NetTime[4] software. The acquisition software recorded the UTC start time of each exposure with sub-second precision.

Image processing and calibration were carried out with the Muniwin software package[5] (Hroch, 2014), which natively supports both file formats. All images were calibrated using dark frames and flat fields obtained with the same ISO settings and exposure times as the corresponding science frames; dark frames were recorded at temperatures closely matching those during the observations. As a final step of the reduction, timestamps were converted to Heliocentric Julian Dates (HJD). Standard aperture photometry was then performed, comparison and check stars were selected, and the resulting light curve was constructed and exported for further analysis.

3. Minima times determination

The times of minima were determined from the observed light curves using the phenomenological modelling approach of Mikulášek (2015). In this method, the eclipse profile is approximated by an analytical function that captures the observed shape of the minimum, and the time of minimum is derived as the model parameter corresponding to the centre of symmetry of the eclipse. Because the fit uses the full eclipse profile rather than only observations near the bottom of the minimum, the resulting timings are generally less affected by observational

[1] https://diffractionlimited.com/product/maxim-dl/
[2] https://astrophotography.app/
[3] https://www.ap-i.net/ccdciel/en/start
[4] https://www.timesynctool.com/
[5] https://c-munipack.sourceforge.net/

scatter and incomplete phase coverage. The phenomenological model describes the eclipse shape reliably without requiring any physical modelling of the binary system, and the minimum time follows directly from the fitted profile. This makes the approach both practical and well-suited to datasets of varying photometric quality.

Uncertainties were estimated using a bootstrap resampling procedure following Cagaš & Pejcha (2012). In contrast to analytical error estimates, the bootstrap method derives timing uncertainty directly from the data and therefore naturally reflects the actual noise level, sampling cadence, and photometric quality of each light curve. This generally leads to more realistic uncertainty estimates for eclipse timings (Cagaš & Pejcha, 2012; Efron, 1979; Davison & Hinkley, 1997). All minima presented in Tab. 3 were determined using the same fitting and uncertainty estimation procedure, which ensures consistency across the entire dataset.

Table 3. DSLR times of minima.

HJD	σ_+	σ_-	Type	Site ID	System
W UMa					
2459655.60271	0.00010	0.00009	p	PO	II
RT And					
2456864.48750	0.00011	0.00012	p	KOL	I
2458133.35155	0.00051	0.00050	s	PO	II
2459749.38491	0.00013	0.00012	p	KOL	III
RW Com					
2459750.39162	0.00022	0.00022	p	PO	II
2460100.47968	0.00020	0.00019	p	KOL	III
RZ Com					
2459403.37043	0.00024	0.00024	s	PO	II
SV Cam					
2457240.53436	0.00020	0.00019	p	KOL	I
2457963.48495	0.00036	0.00035	p	KOL	I
2459595.62033	0.00010	0.00010	p	PO	II
SW Lac					
2458134.25625	0.00011	0.00012	p	PO	II
2459512.38900	0.00006	0.00005	p	PO	II
TV UMi					
2457991.43294	0.00174	0.00132	p	KOL	I
TX Cnc					
2458227.39257	0.00047	0.00046	s	PO	II
2460410.39161	0.00031	0.00032	p	KOL	III
TY Boo					
2459420.34065	0.00129	0.00099	p	PO	II

Table 3. Continued.

HJD	σ_+	σ_-	Type	Site ID	System
2460192.27537	0.00021	0.00018	p	PO	II
TY UMi					
2459803.37993	0.00052	0.00052	p	PO	II
TZ Boo					
2457994.39412	0.00024	0.00024	s	KOL	I
2458360.35199	0.00038	0.00116	p	PO	II
2459742.44251	0.00021	0.00020	p	KOL	III
2460170.35273	0.00038	0.00035	p	PO	II
2460175.40441	0.00036	0.00035	p	PO	II
2460181.34458	0.00044	0.00046	p	PO	II
TZ Lyr					
2459811.55309	0.00074	0.00088	p	PO	II
2459870.25284	0.00017	0.00018	p	PO	II
2459871.31030	0.00015	0.00014	p	PO	II
UV Leo					
2458251.37130	0.00025	0.00029	p	PO	II
UV Lyn					
2459667.41873	0.00038	0.00037	p	PO	II
UX UMa					
2459733.37571	0.00035	0.00026	p	PO	II
2459748.51924	0.00017	0.00015	p	PO	II
2460099.38049	0.00014	0.00012	p	KOL	III
VV UMa					
2460435.46899	0.00120	0.00150	s	PO	II
2460443.37132	0.00024	0.00023	p	PO	II
2460445.43294	0.00012	0.00012	p	PO	II
VW Cep					
2459519.40644	0.00028	0.00030	s	PO	II
2459519.26540	0.00000	0.00056	p	PO	II
VW UMi					
2459782.48803	0.00024	0.00021	p	KOL	III
WZ Cep					
2457973.42104	0.00021	0.00022	s	KOL	I
XY UMa					
2458218.34547	0.00019	0.00021	p	PO	II
2458229.36290	0.00013	0.00014	p	PO	II
2459666.59436	0.00061	0.00059	s	PO	II
YY CrB					
2457996.38787	0.00028	0.00025	p	KOL	I

Table 3. Continued.

HJD	σ_+	σ_-	Type	Site ID	System
AA UMa					
2458230.43093	0.00023	0.00026	p	PO	II
2459664.54883	0.00028	0.00028	s	PO	II
2460006.51446	0.00033	0.00019	p	KOL	III
AB And					
2456858.44583	0.00014	0.00014	p	KOL	I
2457577.48605	0.00015	0.00015	s	KOL	I
2458133.23380	0.00010	0.00009	p	PO	II
AC Boo					
2458379.35665	0.00080	0.00043	p	PO	II
2459782.46884	0.00028	0.00024	p	PO	II
2459783.52443	0.00057	0.00056	p	PO	II
2460070.42200	0.00008	0.00010	p	KOL	III
2460171.38856	0.00043	0.00076	s	PO	II
AD And					
2459873.23762	0.00028	0.00027	s	KOL	III
AH Tau					
2458566.28967	0.00009	0.00028	p	PO	II
AO Cam					
2458218.28395	0.00023	0.00024	p	PO	II
2458230.32697	0.00041	0.00059	s	PO	II
2458532.34742	0.00005	0.00079	p	PO	II
2459656.31230	0.00016	0.00015	p	PO	II
2459657.30118	0.00017	0.00017	p	PO	II
2460005.34342	0.00013	0.00013	p	PO	II
AU Ser					
2456867.37266	0.00012	0.00013	p	KOL	I
2458001.35281	0.00062	0.00044	p	KOL	I
2458374.32056	0.00030	0.00034	p	PO	II
2458375.28801	0.00019	0.00040	s	PO	II
2459763.38642	0.00011	0.00010	p	KOL	III
2459767.44550	0.00022	0.00047	s	PO	II
2460057.31694	0.00019	0.00015	s	KOL	III
AV Del					
2459754.39392	0.00162	0.00152	p	KOL	III
2459781.36786	0.00100	0.00109	p	KOL	III
AX Dra					
2460428.50409	0.00009	0.00009	p	KOL	III
2460429.35302	0.00053	0.00117	s	KOL	III
2460435.32036	0.00011	0.00012	p	KOL	III

Table 3. Continued.

HJD	σ_+	σ_-	Type	Site ID	System
AZ Cam					
2459503.28942	0.00047	0.00045	p	PO	II
BD And					
2459811.47406	0.00025	0.00024	s	KOL	III
BE Dra					
2457967.48118	0.00032	0.00033	p	KOL	I
2458382.34409	0.00008	0.00086	p	PO	II
2460445.42959	0.00038	0.00036	s	KOL	III
2460446.47254	0.00028	0.00028	s	KOL	III
BI CVn					
2459402.41870	0.00057	0.00136	p	PO	II
2460122.43049	0.00025	0.00025	p	KOL	III
BS Cas					
2459797.47612	0.00015	0.00017	p	KOL	III
2460134.42994	0.00014	0.00013	p	KOL	III
2460171.42813	0.00020	0.00018	p	KOL	III
BX Peg					
2456865.37891	0.00013	0.00013	p	KOL	I
2457234.40818	0.00030	0.00028	p	KOL	I
2457580.44201	0.00016	0.00016	p	KOL	I
2457939.51836	0.00014	0.00017	s	KOL	I
2458349.34688	0.00017	0.00029	p	KOL	I
2459504.38520	0.00014	0.00015	p	PO	II
2459513.35839	0.00013	0.00018	p	PO	II
BX Tri					
2459519.61286	0.00127	0.00146	p	PO	II
2459824.55583	0.00033	0.00031	p	KOL	III
2459824.45336	0.00066	0.00075	s	KOL	III
2459826.48193	0.00048	0.00038	p	KOL	III
2459826.38027	0.00055	0.00067	s	KOL	III
2459870.29992	0.00065	0.00070	s	KOL	III
2459870.40264	0.00058	0.00048	p	KOL	III
CC Com					
2459658.58499	0.00026	0.00025	p	PO	II
2460006.38161	0.00011	0.00011	p	KOL	III
2460020.28473	0.00010	0.00012	p	KOL	III
CD Cam					
2456746.39357	0.00056	0.00056	p	KOL	I
CE Leo					
2459726.39758	0.00033	0.00034	p	PO	II

Table 3. Continued.

HJD	σ_+	σ_-	Type	Site ID	System
CG Cyg					
2459516.31537	0.00011	0.00012	p	PO	II
2460176.49246	0.00008	0.00009	p	KOL	III
2460177.44011	0.00014	0.00013	s	KOL	III
2460178.38626	0.00011	0.00012	p	KOL	III
2460181.54189	0.00006	0.00007	p	KOL	III
CW Cas					
2458352.34338	0.00042	0.00004	p	KOL	I
2459595.24635	0.00016	0.00016	p	PO	II
2459817.33219	0.00011	0.00013	s	KOL	III
2459817.49015	0.00008	0.00008	p	KOL	III
2459968.30968	0.00013	0.00013	p	KOL	III
2460135.39130	0.00024	0.00022	p	KOL	III
CW Sge					
2460193.48318	0.00074	0.00073	p	PO	II
DL CVn					
2459728.43894	0.00079	0.00072	p	PO	II
DN Cam					
2459664.38402	0.00018	0.00017	s	PO	II
EF Cep					
2459780.42807	0.00019	0.00019	p	KOL	III
EF Dra					
2457975.45834	0.00040	0.00038	p	KOL	I
2459826.35536	0.00039	0.00036	p	PO	II
2460020.56310	0.00041	0.00045	p	KOL	III
2460181.48457	0.00037	0.00040	s	KOL	III
2460184.45217	0.00069	0.00073	s	KOL	III
2460199.50290	0.00041	0.00046	p	PO	II
EP And					
2458354.35106	0.00050	0.00127	p	KOL	I
2459880.26265	0.00023	0.00021	p	KOL	III
ES UMa					
2460176.40850	0.00085	0.00129	p	KOL	III
FU Dra					
2457582.46906	0.00011	0.00011	p	KOL	I
2457987.34091	0.00015	0.00015	p	KOL	I
2457990.40826	0.00014	0.00014	p	KOL	I
2458371.35560	0.00056	0.00047	p	PO	II
2458378.40967	0.00062	0.00016	p	PO	II
2459402.54875	0.00111	0.00105	p	PO	II

Table 3. Continued.

HJD	σ_+	σ_-	Type	Site ID	System
2459403.46734	0.00116	0.00050	p	PO	II
2459404.54407	0.00046	0.00053	s	PO	II
2459404.38927	0.00051	0.00051	p	PO	II
2459824.44214	0.00017	0.00025	s	PO	II
2460007.39824	0.00018	0.00018	p	KOL	III
2460137.44779	0.00008	0.00008	p	KOL	III
2460184.37482	0.00041	0.00039	p	KOL	III
GW Cep					
2457964.41394	0.00019	0.00020	p	KOL	I
2459652.31220	0.00024	0.00025	p	PO	II
2459653.42913	0.00038	0.00040	s	PO	II
2459746.36691	0.00012	0.00011	p	KOL	III
2459797.38000	0.00009	0.00008	p	KOL	III
2459990.27421	0.00017	0.00025	p	PO	II
2459991.23055	0.00020	0.00026	p	PO	II
2460149.37097	0.00017	0.00016	p	KOL	III
GZ And					
2457977.45556	0.00026	0.00028	s	KOL	I
2458532.27716	0.00031	0.00022	s	PO	II
HH UMa					
2458229.47158	0.00072	0.00069	p	PO	II
2460066.37353	0.00069	0.00076	p	KOL	III
HL Dra					
2459513.27802	0.00055	0.00063	p	PO	II
HW Cam					
2459731.45795	0.00029	0.00026	p	PO	II
2459743.46873	0.00046	0.00045	p	PO	II
LO And					
2458353.33715	0.00051	0.00018	p	KOL	I
MZ Dra					
2460320.30591	0.00023	0.00022	p	KOL	III
NR Cam					
2458223.45928	0.00030	0.00031	s	PO	II
2458223.32773	0.00021	0.00022	p	PO	II
2458348.45628	0.00004	0.00052	p	PO	I
2459652.45368	0.00025	0.00029	p	PO	II
2459652.57780	0.00034	0.00038	s	PO	II
2459656.41577	0.00031	0.00030	s	PO	II
2459657.43953	0.00038	0.00039	s	PO	II
2460004.55036	0.00018	0.00021	p	KOL	III

Table 3. Continued.

HJD	σ_+	σ_-	Type	Site ID	System
2460085.53583	0.00024	0.00026	s	KOL	III
2460085.40876	0.00064	0.00086	p	KOL	III
2460408.46246	0.00022	0.00021	s	KOL	III
2460408.59109	0.00021	0.00019	p	KOL	III
NU Cam					
2459659.53924	0.00090	0.00094	s	PO	II
2459660.57469	0.00055	0.00052	p	PO	II
OT Cep					
2459745.43858	0.00014	0.00015	p	KOL	III
OU Ser					
2457991.31317	0.00046	0.00039	s	KOL	I
PP Lac					
2458350.35329	0.00025	0.00020	p	KOL	I
2459504.50295	0.00022	0.00021	p	PO	II
2460097.42480	0.00015	0.00016	p	KOL	III
V339 Boo					
2459748.41925	0.00040	0.00041	p	KOL	III
2459750.41184	0.00054	0.00046	s	KOL	III
V344 Lac					
2459517.35800	0.00047	0.00050	p	PO	II
V380 Dra					
2459452.48806	0.00039	0.00049	s	PO	II
2459461.37468	0.00031	0.00029	s	PO	II
2459462.36228	0.00059	0.00057	s	PO	II
2459466.31405	0.00029	0.00027	s	PO	II
2459484.33453	0.00020	0.00019	p	PO	II
2459835.38068	0.00024	0.00022	p	PO	II
2459869.44827	0.00009	0.00016	p	KOL	I
V401 Cyg					
2460168.48169	0.00017	0.00014	p	KOL	III
V405 Dra					
2460443.45278	0.00018	0.00018	s	KOL	III
V432 Per					
2458531.39429	0.00054	0.00019	p	PO	II
2460194.56876	0.00010	0.00009	p	KOL	III
V483 And					
2459785.44377	0.00022	0.00025	p	KOL	III
2459818.41690	0.00028	0.00029	p	KOL	III

Table 3. Continued.

HJD	σ_+	σ_-	Type	Site ID	System
V508 Oph					
2458377.35657	0.00031	0.00053	p	PO	II
2459441.38432	0.00006	0.00006	p	VM	III
V523 Cas					
2457581.45014	0.00010	0.00011	s	KOL	I
2457965.52716	0.00007	0.00007	p	KOL	I
2458531.30138	0.00035	0.00016	p	PO	II
2459510.47663	0.00016	0.00016	p	KOL	III
2459816.49977	0.00008	0.00008	s	KOL	III
2459816.38322	0.00007	0.00008	p	KOL	III
2459821.52463	0.00010	0.00011	p	KOL	III
2459821.40714	0.00008	0.00007	s	KOL	III
2459828.30184	0.00007	0.00007	p	KOL	III
2459828.41811	0.00007	0.00007	s	KOL	III
2460141.45233	0.00006	0.00006	p	KOL	III
2460193.33312	0.00007	0.00008	p	KOL	III
V584 Cam					
2459595.41453	0.00053	0.00050	p	PO	II
V608 Cam					
2459681.30569	0.00070	0.00072	s	PO	II
2459684.44106	0.00074	0.00071	s	PO	II
2459736.41993	0.00101	0.00136	s	PO	II
2459758.37596	0.00042	0.00047	s	KOL	III
2459796.45937	0.00042	0.00042	s	KOL	III
2459871.28252	0.00058	0.00060	s	KOL	III
2459912.28431	0.00010	0.00010	p	KOL	III
2460086.35476	0.00031	0.00035	s	KOL	III
V651 Cas					
2459513.44400	0.00007	0.00009	p	PO	II
V728 Her					
2459493.29475	0.00054	0.00056	p	PO	II
2459502.25215	0.00051	0.00050	p	PO	II
2459802.47311	0.00062	0.00066	p	PO	II
2460171.49534	0.00056	0.00052	p	PO	II
V781 Tau					
2459666.26558	0.00023	0.00022	p	PO	II
2459667.29945	0.00024	0.00024	p	PO	II
V829 Her					
2457984.42564	0.00035	0.00029	s	KOL	I
2459799.39132	0.00069	0.00068	p	KOL	III

Table 3. Continued.

HJD	σ_+	σ_-	Type	Site ID	System
2460169.36116	0.00050	0.00039	p	PO	II
2460170.43614	0.00037	0.00035	p	PO	II
2460193.35769	0.00044	0.00044	p	PO	II
V857 Her					
2459504.27549	0.00064	0.00047	p	PO	II
2459779.48032	0.00033	0.00035	p	PO	II
V902 Cep					
2459516.52088	0.00040	0.00039	p	PO	II
2459517.50695	0.00033	0.00032	p	PO	II
2459534.27012	0.00068	0.00073	p	PO	II
2459535.26110	0.00054	0.00051	p	PO	II
2459562.37442	0.00059	0.00053	s	PO	II
2460065.45629	0.00028	0.00024	p	KOL	III
2460143.52164	0.00109	0.00106	s	KOL	III
V955 Cep					
2459502.56360	0.00072	0.00073	p	PO	II
V1018 Cyg					
2459486.45833	0.00096	0.00096	p	PO	II
V1191 Cyg					
2457964.52597	0.00023	0.00025	p	KOL	I
V1297 Cas					
2459783.44089	0.00020	0.00022	p	KOL	III
V1918 Cyg					
2456865.47915	0.00017	0.00021	p	KOL	I
2457957.50619	0.00021	0.00021	p	KOL	I
2459512.29336	0.00027	0.00025	p	PO	II
2459517.24954	0.00020	0.00018	p	PO	II
2459866.38306	0.00022	0.00019	p	PO	II
2460075.45112	0.00010	0.00011	p	KOL	III
V2277 Cyg					
2459502.37053	0.00015	0.00020	p	PO	II
NSVS 5789962					
2459461.46165	0.00174	0.00399	p	PO	II
2459466.56294	0.00169	0.00464	s	PO	II

Notes. p and s denote primary and secondary minima, respectively. The columns Site ID and System correspond to Tab. 2 and 1, respectively.
The computer readable form of these data can be found at: `https://www.astro.sk/caosp/Eedition/FullTexts/vol56no3/pp68-82.dat/`.

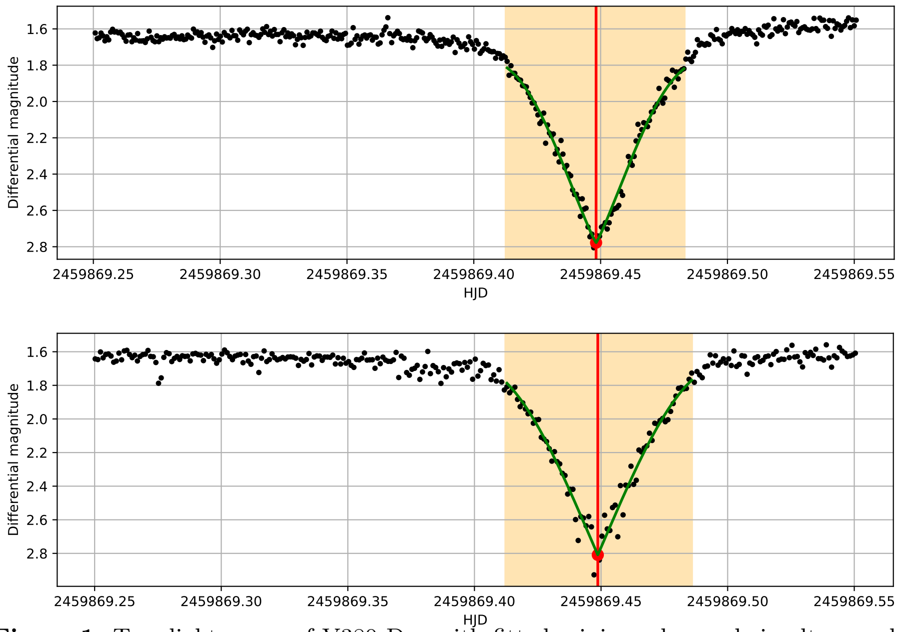

Figure 1. Two lightcurves of V380 Dra with fitted minima observed simultaneously from Kolonica saddle (above) and from Prešov (bottom).

4. Limitations

Several sources of measurement uncertainty are inherent to the use of a DSLR camera as a photometric detector. These include the presence of the Bayer filter array, a lower bit depth compared to dedicated CCD and CMOS cameras, and the absence of sensor cooling, which leads to higher dark current and increased thermal noise — particularly during observations at elevated ambient temperatures. The quantum efficiency of DSLR sensors is also generally lower than that of purpose-built astronomical detectors. Beyond the instrument itself, the observations were acquired under varying conditions, including sites affected by moderate light pollution and changing atmospheric transparency. The observations were also affected by varying atmospheric seeing, although it was not monitored systematically and did not represent a significant limitation for the relatively bright targets included in this study.

To illustrate the effect of observing conditions on DSLR photometry, the same minimum of V380 Dra was observed simultaneously from two sites using different telescope systems: one from Kolonica Saddle within the Dark Sky Park Poloniny, and the other from the urban environment of Prešov (Fig. 1).

As expected, the light curve from the dark-sky site shows noticeably lower point-to-point scatter and a smoother eclipse profile. The urban observation, by contrast, exhibits increased photometric noise, reflecting the combined effect of a brighter sky background, a smaller telescope aperture, and higher detector gain settings. These differences are visible both in the precision of individual measurements and in the uncertainties of the derived eclipse timings (Tab. 4).

Despite the substantially different observing conditions, both datasets produced mutually consistent times of minimum. This comparison shows that DSLR-based eclipse timing remains feasible even in the presence of significant light pollution. While dark-sky observations naturally yield better photometric quality and more precise timing determinations, urban sites can still contribute scientifically useful eclipse timings suitable for long-term period monitoring of eclipsing binaries. For our final compilation, we adopted the timing value derived from the Kolonica Saddle observations.

Table 4. Comparison of two independent observations of the eclipse minimum of V380 Dra obtained under different observing conditions.

Parameter	Kolonica Saddle	Prešov
Site type	Dark-sky site	Urban site
SQM (mag arcsec^{-2})	21.89	20.26
Telescope	Newton 200/1200	APO 102/500
Exposure time (s)	30	60
ISO	800	1800
Point error (mag)	0.005–0.008	0.013–0.016
HJD minimum	2459869.448266	2459869.448703
σ_{-} (d)	0.0000933	0.0002160
σ_{+} (d)	0.0001567	0.0001904

5. Discussion and Conclusions

We have presented a collection of 250 new times of minima for 86 eclipsing binary systems, obtained between 2014 and 2024 using DSLR photometry. All timings were derived from uniformly reduced observations and determined using a consistent fitting and uncertainty estimation procedure, ensuring homogeneity across the entire dataset. The results confirm that DSLR cameras can provide eclipse timings with sufficient precision for many practical applications in eclipsing binary research. While such detectors cannot fully match the performance of modern dedicated CCD and CMOS cameras, they remain a viable and accessible option for long-term photometric monitoring. We have also shown that useful eclipse timings can be obtained not only from dark-sky sites but also from locations affected by moderate light pollution, thereby broadening the potential contribution of amateur and semi-professional observers to this type of systematic monitoring.

The timings presented here extend the available observational coverage of the studied systems and may serve as useful input for future investigations of orbital period variations and other long-term phenomena in eclipsing binaries.

Acknowledgements. The Slovak Research and Development Agency supported this work under contract no APVV-24-0160. M.K. was supported by the internal grant No. VVGS-2025-3480 of the P.J. Šafárik University in Košice.

References

Applegate, J. H., A Mechanism for Orbital Period Modulation in Close Binaries. 1992, *Astrophysical Journal*, **385**, 621, DOI:10.1086/170967

Borkovits, T., Rappaport, S., Hajdu, T., & Sztakovics, J., Eclipse timing variation analyses of eccentric binaries with close tertiaries in the Kepler field. 2015, *Monthly Notices of the RAS*, **448**, 946, DOI:10.1093/mnras/stv015

Cagaš, P. & Pejcha, O., Discovery of a double eclipsing binary with periods near a 3:2 ratio. 2012, *Astronomy and Astrophysics*, **544**, L3, DOI:10.1051/0004-6361/201219815

Davison, A. & Hinkley, D., Bootstrap Methods and Their Application. 1997, *Journal of the American Statistical Association*, **94**, DOI:10.2307/1271471

Efron, B., Bootstrap Methods: Another Look at the Jackknife. 1979, *The Annals of Statistics*, **7**, 1 , DOI:10.1214/aos/1176344552

Gimenez, A. & Garcia-Pelayo, J. M., A New Method for the Analysis of Apsidal Motions in Eclipsing Binaries. 1983, *Astrophysics and Space Science*, **92**, 203, DOI:10.1007/BF00653602

Hroch, F. 2014, Munipack: General astronomical image processing software, Astrophysics Source Code Library, record ascl:1402.006

Irwin, J. B., The Determination of a Light-Time Orbit. 1952, *Astrophysical Journal*, **116**, 211, DOI:10.1086/145604

Kamenec, M., Transformation of DSLR magnitudes to standard photometric system. 2023, *Open European Journal on Variable Stars*, **243**, 1, DOI:10.5817/OEJV2023-0243

Loughney, D., Variable star photometry with a DSLR camera. 2010, *Journal of the British Astronomical Association*, **120**, 157

Mikulášek, Z., Phenomenological modelling of eclipsing system light curves. 2015, *Astronomy and Astrophysics*, **584**, A8, DOI:10.1051/0004-6361/201425244

Watson, C., Henden, A., & Price, A., The International Variable Star Index (VSX). 2007, *Journal of the American Association of Variable Star Observers (JAAVSO)*, **35**, 414

Zhang, M., Bakos, G. Á., Penev, K., et al., Precision Multiband Photometry with a DSLR Camera. 2016, *Publications of the ASP*, **128**, 035001, DOI:10.1088/1538-3873/128/961/035001